IOP Publishing Physiol. Meas. 40 (2019) 014002 (13pp) https://doi.org/10.1088/1361-6579/aaf089

Physiological Measurement

IPEM Institute of Physics and Engineering in Medicine

PAPER

Network physiology of 'fight or flight' response in facial superficial blood vessels

RECEIVED
5 July 2018

REVISED
5 November 2018

ACCEPTED FOR PUBLICATION
13 November 2018

PUBLISHED
21 January 2019

Amin Derakhshan[1], Mohammad Mikaeili[1,3], Ali Motie Nasrabadi[1] and Tom Gedeon[2]

[1] Biomedical Engineering Department, Shahed University, Tehran, Iran
[2] Human-Centred Computing Research Group, Research School of Computer Science, Australian National University, Canberra, Australia
[3] Author to whom any correspondence should be addressed.

E-mail: a.derakhshan@shahed.ac.ir, mikaili@shahed.ac.ir, Nasrabadi@shahed.ac.ir and tom.gedeon@anu.edu.au

Keywords: effective connectivity, facial thermal imaging, Granger causality, fight or flight resposne, graph analysis, network physiology

Abstract

Objective: We introduced a novel framework to identify the dynamic pattern of blood flow changes in the cutaneous superficial blood vessels of the face for 'fight or flight' responses through facial thermal imaging. *Approach*: For this purpose, a thermal dataset was collected from 41 subjects in a mock crime scenario. Five facial areas including periorbital, forehead, perinasal, cheek and chin were selected on the face. Due to the cause and effect movement of blood in the facial cutaneous vasculature, the effective connectivity approach and graph analysis were used to extract causality features. The effective connectivity was quantified using a modified version of the multivariate Granger causality (GC) method among each pair of facial region of interests. *Main results*: Validation was performed using statistical analysis, and the results demonstrated that the proposed method was statistically significant in detecting the physiological pattern of deceptive anxiety on the face. Moreover, the obtained graph is visualized by different schemes to show these interactions more effectively. We used machine learning techniques to classify our data based on the GC values, which result in a greater than 87% accuracy rate in discriminating between deceptive and truthful subjects.

1. Introduction

When potential danger is perceived, the brain should decide between two primary solutions to survive: fight or flight (Jacobs 2001). Physical and mental threats activate the fight or flight response in the same way and there is no substantial difference between them (Wilhelmsen 2000). The emotions that are related to this physiological reaction such as anger or fear are controlled by a 'primitive' part of the brain called the amygdala. Since there is no connection from the prefrontal cortex (which controls the conscious and decision-making processes) to the amygdala, and since there are so many pathways from the amygdala to the cortex, the level of consciousness in these situations is insignificant (LeDoux 2007). Therefore, the physiological response to the threat is essentially controlled by the amygdala. It is known that the amygdala, as a part of the limbic system, activates the sympathetic nervous system while sending information to the hypothalamus (Lacroix 2000). The hypothalamus is of fundamental importance for the control of ACTH secretion and hence for the adrenal cortex and corticosterone secretions that regulate vasoconstriction and vasodilation in different parts of the body (Buijs 2000).

One of the first rigorous experimental analyses of temperature changes on the face after emotional stimulation has pointed out that this mechanism can be observed on the face by a high-sensitivity infrared thermal camera (Pavlidis and Levine 2002). The subjects started the experiment in a quiet room with low light to create a calming environment. Then, without any notice, the participants were startled with a loud sound while their faces were monitored with a thermal imager. By comparing before and after the startle, it was found that there is a temperature increase in the periorbital region. Since the measured temperature change was so quick and occurred in less than 300 ms, in controlled environmental conditions it was concluded this is the result of the fight or flight mechanism on the cutaneous vasculature. In another investigation evaluating different regions of interest (ROIs) on the face, different patterns of temperature changes before and after stress stimulation were reported (Shastri *et al* 2009). It was found that blood redirects from some areas on the face that require less blood,

for example the cheek and nose, to ROIs that need more, for example the periorbital muscle that needs to contract more due to faster eye movements during threatening situations.

One of the most significant discussions in this area is the validity of facial thermal imaging as an indirect method to detect blood flow in the cutaneous facial blood vessels. To this date, laser Doppler is considered the gold standard method for quantifying the microvascular cutaneous blood flow and it can be used to evaluate the performance of thermal imaging. A comparative study showed that thermal imaging is linearly correlated (Pearson correlation = 0.85) with laser Doppler imaging (Merla *et al* 2008). In another major study, Puri collected thermal videos of the forehead area in addition to the oxygen consumption rate (for measuring energy expenditure) of 12 subjects. He showed that there is a high correlation (Pearson correlation = 0.91) between the maximum temperature of the forehead area and oxygen consumption rate, which is an indicator of stress (Puri *et al* 2005). The perinasal response to stress stimuli was shown to be well correlated with the transient perspiratory response on the fingers (Pavlidis *et al* 2012).

There is very little previous literature on the physiological mechanism of stress response in the facial superficial vasculature. Some research findings on the importance of the periorbital area have not been consistent with those of Pavlidis *et al* (2000). For instance, Yuen and his team used nine volunteers for a mathematical calculation experiment and found there was an increase in the overall temperature of the face during their experiment that was mostly caused by the forehead, lips and ears (Yuen 2009). Furthermore, in a study that replicated the protocol of Pavlidis with 24 subjects and chose periorbital, cheek and carotid as the ROIs, the results indicated that the periorbital area seems not to be as important as the cheek area in a deception detection approach (Pollina *et al* 2015). These experimental observations and results suggest a hypothesis that there is a special pattern for each type of emotion, reflecting the physiological and anatomical variations following an affective stimulation. These physiological patterns can be investigated by thermal image acquisition and analysis of the human body, especially the face, and could lead to better understanding of underlying physiological mechanisms. As a specific example, it is still uncertain what the effect of the fight or flight response is on the temperature distribution and superficial blood flow changes on the face.

Network physiology as a new interdisciplinary field has emerged to investigate the complex network and dynamic behavior among integrated physiological systems and subsystems (Ivanov *et al* 2016). This approach focuses on the question of how physiological interactions can be assessed and analysed through an integrative network framework where graph theory is utilized to extend our knowledge about the inherent physiological mechanism as a non-linear, non-stationary and spatio-temporal scale system. This approach has led to some interesting outcomes about the statistical evaluation of organ dysfunction like sepsis (Moorman *et al* 2016) and multiple organ failure (Buchman 2006). All previous research in this field has focused on neural connections among various organs after a stimulation or during a disease activation. As far as we can find, there is no published literature or study on blood flow or temperature time series as a consequence of neural activation and its use in studying the inherent nature of their interactions.

In this paper we propose a novel methodology by effective connectivity analysis, to investigate the physiological blood and temperature redistribution following fight or flight responses. This kind of connectivity approach has been widely used in EEG and fMRI time series analysis for different psychological disorders (Seth *et al* 2015). In our study, we considered facial ROIs as our nodes (instead of the brain regions used in other studies) and the temperature distribution pattern over the face as the connectivity information. Note that the vascular and nervous branch structures are partly similar: in the vasculature the carrier is blood, and in the neural system it is action potential. Further, the speed of blood flow changes following activation of the sympathetic nervous system is very quick (Pavlidis *et al* 2000), therefore the same methodological procedure can be chosen for these two different natures (neural and vascular) connections. We modelled this connectivity by weighted directed graph analysis, in which nodes are the ROIs on the face and the links are the causal connections between ROIs.

This paper suggests 'effective connectivity' for investigating the effect of fight or flight responses on blood flow changes between different ROIs on the face. A dataset for this study was collected by facial thermal imaging of 32 subjects in a mock crime interrogation. By extracting the Granger causality (GC) values which consider the instantaneous interactions between five ROIs on the face, we examined the effective connectivity between them and visualized these causalities by graph representation techniques. We also employed four feature selection methods and four classification models to evaluate the power of these features to discriminate between deceptive and truthful subjects. Furthermore, other measures such as sensitivity, specificity, precision and F-score were used to show the performance of the utilized classifiers. The results indicate the effective utilization of these machine learning techniques.

2. Experimental setup

We collected our experimental data using a mock crime protocol, in which the participants were divided into two groups: deceptive and truthful. The deceptive participant entered a crime room and 'stole' a gold necklace

from a locked drawer using some keys that they easily 'found' in the room. The truthful subjects left the room without being instructed to perform any 'criminal' act. All of the subjects were brought to an interrogation room where the interviewer asked eight yes/no questions based on the comparison question test (CQT) protocol (Ben-Shakhar 2002). The questions were categorized as Relevant, Irrelevant and Neutral questions, in which the deceptive subjects were asked to deceive the interviewer in questions relevant to deception. A software was developed to manage the question and answer timeline. The questions were as follows.

1. Do you live in Tehran?
2. Do you intend to answer all the questions honestly?
3. Have you ever checked your sister's/brother's phone without her/his consent?
4. Did you enter the office at the back of the building?
5. Do you have any plan after this interview?
6. Did you steal the necklace?
7. Would you be happy if our device does not work properly?
8. Is there any other question that could make you anxious?

Meanwhile, their psycho-physiological signs were monitored using facial thermal imaging. For our research, we used a FLIR T640 thermal camera. The camera had an uncooled and stabilized microbolometer detector with a maximum focal plane array (FPA) resolution of 640 × 480. The thermal sensitivity was 35 mK at 30 °C and the frame rate was set to 10 fps in all our recordings.

The experiment included 41 participants, but one subject's data was removed from our dataset for data recording technical issues, as the thermal data was corrupted. They were aged 18–35 with equal gender distribution (20 males and 21 females), and with a mean age of 24.4 years with a standard deviation of 3.5 years. The subjects were undergraduate and postgraduate students in Tehran, Iran. The experiment was conducted according to the Helsinki Declaration on proper treatment with human subjects. All the participants completed an informed-consent form upon arrival and they were assigned to the two groups randomly. Furthermore, they were asked to complete another form to declare any current health conditions that could affect their emotional responses, including using any medication in the previous 24 h. They were informed of the procedure of the experiment by printed instruction and also by verbal explanations from the experimenter.

3. Methods

Our main objective is to find a graph representation that effectively shows the psycho-physiological mechanism of the fight or flight response on bloodstream regulation over the face. Specifically, we employed the well-known 'effective connectivity' method (Friston 2011) and graph analysis for visualization. The weighted directed graph representation of this mechanism was validated by an ANOVA statistical test, which showed that the extracted Granger features were statistically significant. Figure 1 illustrates an overview of the study architecture that was developed and is presented in this paper.

3.1. ROI segmentation

To extract the information of any specific emotional state, we selected some ROIs on the face that were most likely to correlate with the emotional states in which we were interested. Appropriate ROI selection is a very challenging issue in the psycho-physiological application of facial thermal imaging. Some studies in the deception detection framework have used the periorbital region as their targeted area on the face (Tsiamyrtzis 2007, Rajoub and Zwiggelaar 2014, Derakhshan 2014). On the other hand, other studies used different ROIs like the cheek region, which they found to contain higher information capacity in comparison to the others (Pollina *et al* 2015).

In this study, we investigated the blood flow connectivity between different regions on the face. The ROIs were selected manually based on the previous studies in this field (Ioannou and Merla 2014) and the anatomy of facial cutaneous blood supply. It is known that the bloodstream in facial skeletal muscles is supplied through two major branch arteries of the carotid artery: the external carotid artery (ECA) and the internal carotid artery (ICA). Facial, maxillary and superficial temporal arteries are three branches of ECA that supply the lower part of the face including nose, lips, chin, cheeks and neck areas. Besides, the upper areas on the face such as the periorbital region and forehead are mostly supplied by the ophthalmic artery that is a branch of the ICA (Prendergast 2013). Therefore, the most important areas on the face can be categorized as perinasal, chin, cheeks, periorbital and forehead. The approximate position of each ROI used in this study is shown in figure 2.

Unwanted head movements were compensated by the Viola–Jones algorithm for face detection (Viola and Jones 2001) and Kanade–Lucas–Tomasi (KLT) method for finding feature points on the face and tracking them continuously in each facial thermal video (Tomasi and Kanade 1991). For each ROI, we computed the maximum temperature value in each frame, which created the temperature signal. Since the selected regions are highly

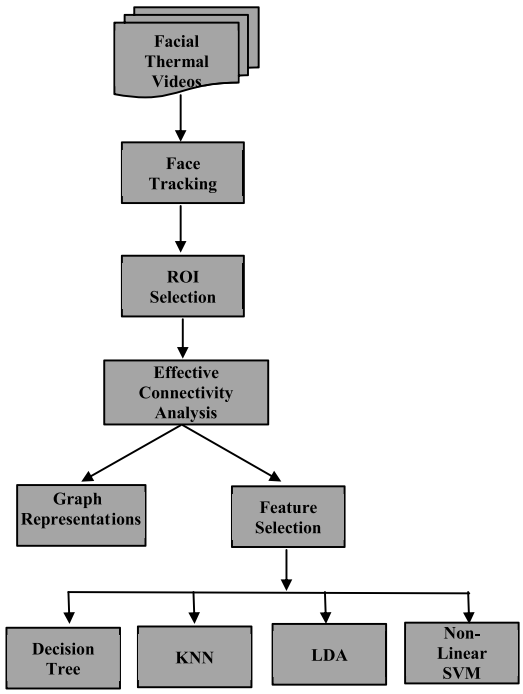

Figure 1. Overview of the methodology in this study. The collected facial thermal videos were tracked and the maximum temperature values in each ROI created a thermal time series. Five thermal time series regarding periorbital, forehead, cheek, perinasal and chin areas were extracted respectively. Effective connectivity between these time series were computed by an extended version of the GC approach and provided input to four linear and non-linear classifier models. Furthermore, the graph measurement and representation of these connectivity values were demonstrated by different templates.

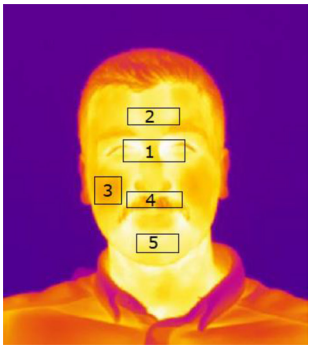

Figure 2. The ROIs that were segmented based on the anatomy of human facial vasculature including periorbital (1), forehead (2), cheek (3), perinasal (4), and chin (5).

enriched in blood vessels, this thermal signal correlates with the blood flow fluctuations in the cutaneous facial vasculature. We normalized all values to [0 1] by the Min-Max normalization method for data uniformity.

After calculating the maximum temperature signal for all ROIs on the face, we used a rlowess[3] smoothing filter (Jacoby 2000), a robust non-parametric regression method, to suppress any high-frequency fluctuations in the temperature signal due to imperfection in the face tracking. This filter is highly effective, especially when the signal contains outliers that is similar to our case. By the end of this process, we had five temperature signals which represent the temperature variations on the important vascular regions of the face.

3.2. Effective connectivity analysis and graph measurement

Study of brain connectivity networks provides an opportunity for the neuroscientist to develop their knowledge of brain function in various disorders. There are three types of connectivity in brains. The first one studies the existence of anatomical integration connecting areas of the brain (structural connectivity); the second refers to the correlation among different regions (functional connectivity); and the third is the causal interactions which exist between those regions (effective connectivity). The analysis of effective connectivity investigates the directed

[3] Robust locally weighted scatterplot smoothing.

influence of each neuron group on the others by a recorded BOLD[4] time series. In recent years, multivariate GC has been widely employed to assess directional influence between two or more time series in neuroscientific studies (Deshpande and Hu 2012, Friston *et al* 2013, Bellucci 2017). It was first introduced by Granger (1969) in terms of vector auto regressive (VAR) modelling of multivariate processes. GC is an increasingly popular approach for estimating the causality among paired time series. However, there are some studies in neuroscience which shows that neglecting the instantaneous effect of physiological variables might lead to misrepresentation of directed paths (Smith 2011). By utilizing methods which consider the contemporaneous causal interactions in addition to the lagged values, they could better return a simulated fMRI dataset (Ramsey 2014, Henry 2017).

In this study, we computed an extended version of the GC algorithm (Schiatti *et al* 2015) in all our recorded thermal time series, to assess the blood flow changes due to fight or flight responses in different facial ROIs. This method has been successfully used for finding network physiology (Duggento 2016, Porta and Faes 2016, Ren 2017). We used thermal times series, which represents the blood flow changes and reflects the physiological mechanism of this phenomenon (fight or flight response).

3.2.1. Extended Granger causality (eGC)

Based on the basic concept of GC, assume that we have two time series, X and Y, and we try to predict the future terms of X based on the past data from X and Y. We can consider Y as the cause of X if the past term of Y would be useful for predicting the future term of X (Bressler and Seth 2011). The procedure for calculating the GC between each pair of ROI temperature signals is described below.

- The VAR model for X that depends only on previous terms of itself can be written as (1)

$$X(t) = \sum_{j=1}^{p} A(j)\, X(t-j) + \varepsilon(t). \tag{1}$$

- The MVAR model for the dependency of X on its own past plus the past terms of Y is

$$X(t) = \sum_{j=1}^{p} A_1(j)\, X(t-j) + \sum_{j=1}^{p} A_2(j)\, Y(t-j) + \varepsilon'(t) \tag{2}$$

where A is the model coefficient, $\varepsilon(t)$ is the prediction error and p is the model order.

- Then, the GC ($\mathcal{F}$) between Y and X is

$$\mathcal{F}_{Y\to X} = \ln \frac{\mathrm{var}(\varepsilon)}{\mathrm{var}(\varepsilon')}. \tag{3}$$

Although GC is a popular method for inferring the causality between paired nodes, there are some shortcomings and drawbacks which could limit the application of GC in physiological computing. Some of the literature has showed that without considering instantaneous causal effects, GC can lead to erroneous conclusions of causality in physiological systems. The main issue is the interference between time-lagged and zero-lagged effects in the VAR model, which has been addressed in both time domain and frequency domain analysis previously (Hyvärinen *et al* 2010, Faes and Sameshima 2014). Thus, they utilized both time lagged and instantaneous (no-delayed) effects as an extended version of GC derived from an extended version of VAR model which accounts for zero-lag effects in linear regressions (Porta and Faes 2016):

$$X(t) = \sum_{j=0}^{p} B(j)\, X(t-j) + W_j(t) \tag{4}$$

$$X(t) = \sum_{j=0}^{p} B_1(j)\, X(t-j) + \sum_{j=0}^{p} B_2(j)\, Y(t-j) + W_j'(t) \tag{5}$$

[4] Blood oxygenation level-dependent.

Table 1. Comparison of different MVAR model order regarding their BIC values. The larger the absolute value of BIC, the better the model according to this criterion.

Model order	1	2	3	4	5
BIC value	−6880	−7005	−7067	−6913	−6791

where $B(j)$ is the new model coefficient based on the extended version of GC. To estimate the eGC, we need to compute the zero-lagged effect among each pairwise timeseries, which is a complicated process compared to traditional GC. For this purpose, we employed a two-step procedure to identify these interactions, which was previously proposed and utilized by Schiatti and her colleagues, effectively (Schiatti *et al* 2015). First, we investigated any effects between $X(t)$ and $Y(t)$ by computing their partial correlation matrix through the inverse of the covariance matrix (Marrelec *et al* 2006). Then, we used pairwise likelihood ratios for non-Gaussian data to identify the direction of the zero-lagged effect among each pairwise time series (Hyvarinen and Smith 2013). The eGC then can be obtained by equation (6):

$$\mathrm{eGC}_{Y\to X} = \ln \frac{\mathrm{var}(W_j(t))}{\mathrm{var}(W'_j(t))}. \tag{6}$$

The model order was chosen as three based on the Bayesian information criterion (BIC) (Rissanen 1989) model selection procedure. The BIC values for different model orders are reported in table 1. Another reason in choosing this model order is that since the frame rate of the thermal camera was set to 10 Hz, and the minimum natural time to respond to the stimulation of the sympathetic nervous system is about 300 ms (Pavlidis *et al* 2000, Gane *et al* 2011), the optimum model order is three.

The GC indexes were normalized to [0 1] for each person by the Min-Max normalization technique. Finally, the normalized GC between each pair of five ROIs creates a 5×5 weighted directed graph for each subject. The values on the main diagonal of this matrix are the self-causality, which is not relevant to us here, so these values were replaced by zero.

3.2.2. Node strength

One of the main advantages of graph analysis is the quantification of network features, which can be useful for improving the pattern recognition and graphical representations phase. Node strength is a type of graph parameter that could be useful in this case (Bullmore and Sporns 2009). The node strength can be calculated by summing up all the path weights that are connected to a node ($S_i = \sum_j W_{ij}$). This parameter provides an excellent way to show the importance of each node (ROI) as an ingoing or outgoing node. More ingoing links is associated with increasing temperature and blood flow in that specific node, which could correspond to the mechanism of fight or flight response on the face.

3.3. Feature evaluation and ranking

To summarize the feature extraction section, based on the CQT protocol, the eight yes/no questions during the mock crime interrogation were recorded and the thermal data related to the relevant questions were segregated from the others. The effective connectivity between each paired node (ROI) was extracted over the time by the extended version of the GC approach, which created 20 features for 31 subjects' thermal videos and five ROIs on each face. This feature vector represents the causal interactions of facial cutaneous blood flow changes related to deceptive behaviour. However, not all these features were discriminative or contained information regarding our protocol.

Feature selection is the process of ranking all features and selecting a subset using an independent evaluation criterion for binary classification of our dataset. This process results in reducing the dimensionality problem and maximizing the classification accuracy rate. In this study, the significance of each feature, based on the discrimination power to separate our two groups, were examined through four evaluation criteria. We chose absolute value of paired sample *t*-test (Li *et al* 2006), relative entropy (Kullback–Leibler divergence) (Kullback 1987), receiver operating characteristic (ROC) (Fawcett 2006) and two-sample unpaired Wilcoxon test (Mann–Whitney) (Kirk 2007) to rank the GC feature set. The MATLAB Bioinformatics toolbox (Henson and Lucio 2004) was used to apply the above feature evaluation criteria.

3.4. Deception classification

We assessed the causality features by their discrimination performance to evaluate the features that were extracted by classification accuracy rate. A feature vector containing 20 paired effective connectivity features was used to train four classifiers, including decision tree, K-nearest neighbourhood (KNN), linear discriminant analysis (LDA) and support vector machine (SVM). For the decision tree classifier, the depth of trees is controlled by the maximum number of splits, and this was set to 10. For KNN, we used five neighbours, and for the SVM

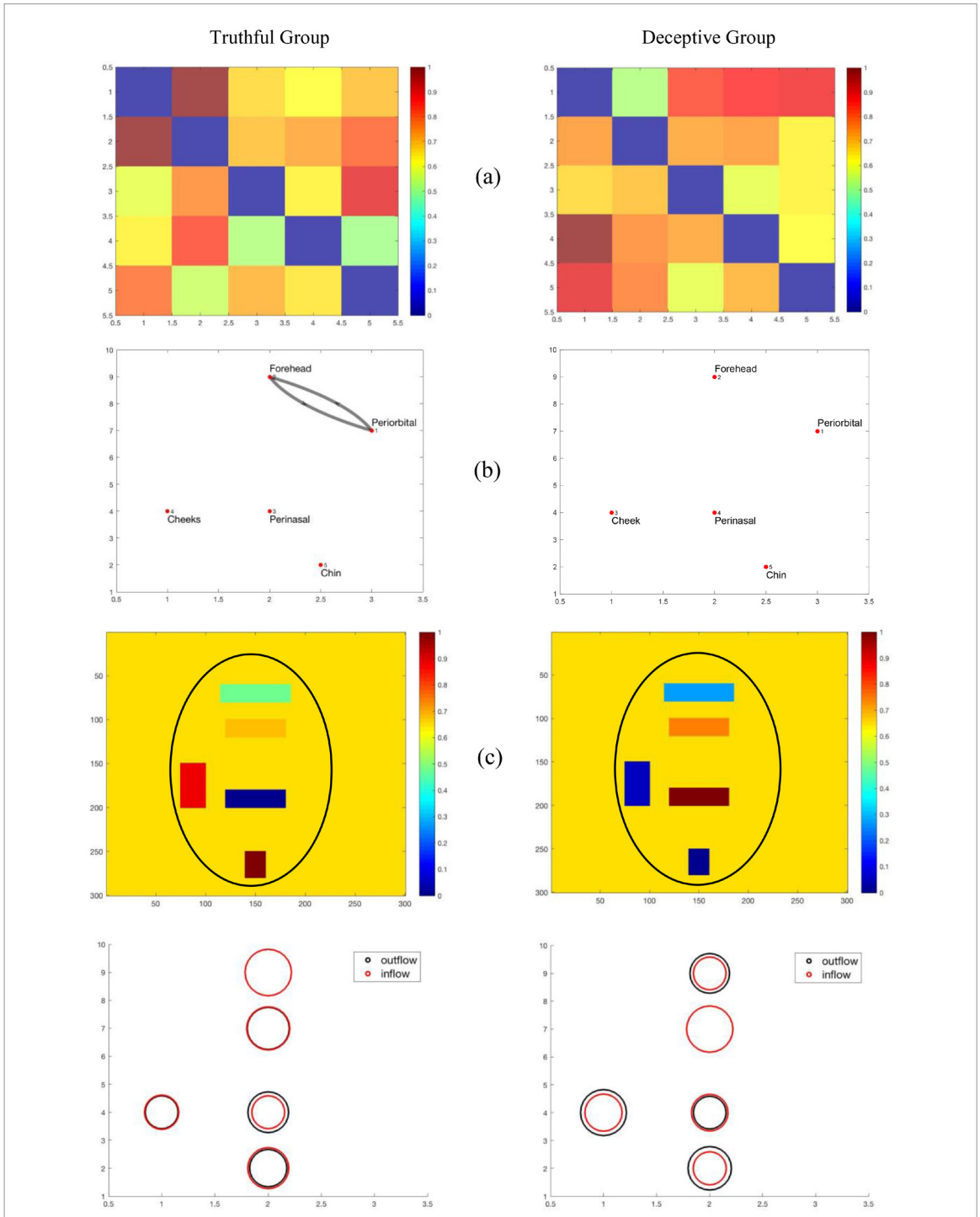

Figure 3. Three visualization schemes for effective connectivity weighted directed graph. The left column is for truthful subjects and the right one is related to deceptive subjects. The node sequence is based on the ROI sequence explained in section 3.1. (a) 5×5 matrix contrast-coded diagram: dark colours represent low values and bright colours higher weights. (b) Node-link diagram showing the highest weights in all paths. (c) Facial ROIs with contrast coded representation of each node, averaged over all subjects. (d) Average of information inflow and outflow for all subjects in each deceptive and truthful group, separately. The diameter of the circles represents the strength of flow. Red circles denote the inflow and black circles indicate outflow of temperature in five regions on the face. The sequence of ROIs is the same as (c).

we used linear and polynomial kernels where the polynomial degree controls the complexity of the mapping space. The default value is 3 and it is generally considered suitable for most cases. Increasing the degree could lead to better classification accuracy for the training data, however it can also cause overfitting issues. Furthermore, to assess how the result of machine learning techniques will generalize to an independent new dataset, we used leave-one-out cross validation. In this method, all the subjects' thermal data except one were used for training the classification model and the single observation was used for testing the performance of the learning algorithm. This process was iterated for the size of our dataset and the final classification result is the average of predicted labels for all subjects.

4. Results and discussion

4.1. Graph representation

To show the 'effective connectivity' patterns among the two group participants, we employed common visualization techniques which had been successfully used in brain connectivity analysis previously. Considering that there were five nodes and 20 links, network reduction was applied to distinguish which ROIs and connections were most involved in fight or flight responses. For effective representation of these causal interactions and their differences between groups, we summed up all the causality values for deceptive and truthful subjects, respectively, which resulted in a 5×5 matrix for each group. Figure 3(a) shows the colour-coded visualizations of these two weighted directed graphs in which the ROIs are the nodes and their averaged strength for all subjects after normalization were visualized by colour shades. It shows some significant differences between the groups: as in the deceptive category the values in the right part of this scheme are much lower than the left part, which shows the temperature information flow from the lower ROIs on the face to the upper ROIs. This supports the previous studies in the field, which indicate that blood moves to the forehead and periorbital areas after fight or flight affective stimulation (Zhu *et al* 2007).

Table 2 reports the mean and standard deviation values of GC matrixes for all subjects in deceptive and truthful groups, separately. To emphasize the links with higher weights, the two highest averaged weights for all subjects in all paths are shown in the form of a node-link diagram in figure 3(b). The edge weights are encoded by the thickness of arrows. As the figure shows, in the deceptive group the direction of the vectors is toward the periorbital area, while in the truthful group no meaningful direction can be observed. The importance of chin $\rightarrow$ periorbital and perinasal $\rightarrow$ periorbital in the deceptive group and the interaction of periorbital and forehead in the truthful group can also be seen in figure 3(a). The node strength values were calculated for each group (deceptive or truthful) and normalized and encoded by colour shades in five rectangles corresponding to five selected ROIs on the face in figure 3(c). It can be inferred from this figure that there are clearly opposite interactions of perinasal–cheek and perinasal–chin in deceptive and truthful subjects. Furthermore, the role of the periorbital area as a destination of blood flow and temperature is more pronounced.

We identified the total information inflow and outflow to estimate the interactions of ROIs with each other. The information inflow was obtained by the sum of all edge weights which direct the information from all other ROIs, or the total information which was received by a ROI. Similarly, the outflow information was obtained by the total information directed toward other ROIs. We represented the inflow and outflow values by the diameter of red and black circles in figure 3(d). In the deceptive group, the higher outflow temperature for the cheek and chin ROIs can be seen, which define the moving out of the blood and dropping the temperature in these regions.

4.2. Validation

To evaluate the causal interaction among each pair of ROIs, a two-tailed t-test between the two groups was performed. The results show that there were four paths with a p value less than 0.05 (table 3). In this table, the path weight deceptive (PWD) refers to eGC values that were averaged over our deceptive group and the path weight truthful (PWT) refers to mean causality indexes for the truthful group. The directionality of the effective connectivity was indicated in the first two columns. The first column is the source ROIs from which the temperature fluctuations affect the ROIs that are listed in the second column. We found that the overall directionality on the face is from the lower region ROIs, such as the chin, to the upper region ROIs, such as the periorbital region and forehead. Moreover, a significant interacting activation of the forehead and periorbital areas can be observed in this table. However, the causal connectivity of the forehead to periorbital ROIs is stronger than the other directions.

4.3. The most discriminative features

Table 4 lists the output of the feature ranking phase. The first row is the feature with the highest discriminative power, and the last row is the worst feature. We utilized four feature ranking methods including t-test, relative entropy, ROC and Wilcoxon test to compare them and to find the best approach for discrimination of deception and truthfulness based on our CQT protocol. The dominance of forehead to periorbital and chin to cheeks stands out in table 4 as the highest ranked feature by all four feature selection methods.

The results of classification are reported in figure 4 and, as is shown there, the decision tree achieved the highest performance of discrimination in classifying deception from truthfulness. The mean accuracy rate was 67.7, with a standard deviation of 0.47. Besides the classification performance that was shown for all features, we executed the same classification procedure for the selected features set, which was ranked by the relative entropy method. We selected the best two features from all four feature ranking methods, and the results indicate an effective utilization of feature selection in improving the accuracy for discrimination of truthful and deceptive subjects. Closer inspection of the results shows the highest classification rate was obtained by SVM with linear kernel, which achieved 87.1% for the selected features ranked by relative entropy method.

Table 2. The mean and standard deviation parameters of eGC values.

	Truthful		Deceptive	
Link	mean	std	mean	std
FH → PO	0.574	0.108	0.395	0.074
CK → PO	0.340	0.065	0.339	0.048
PN → PO	0.365	0.063	0.530	0.114
CN → PO	0.455	0.066	0.465	0.066
PO → FH	0.579	0.102	0.274	0.026
CK → FH	0.443	0.117	0.374	0.098
PN → FH	0.483	0.058	0.391	0.085
CN → FH	0.322	0.043	0.425	0.054
PO → CK	0.383	0.045	0.432	0.090
FH → CK	0.399	0.047	0.411	0.083
PN → CK	0.303	0.030	0.394	0.060
CN → CK	0.411	0.055	0.332	0.067
PO → PN	0.354	0.079	0.458	0.092
FH → PN	0.421	0.076	0.365	0.079
CK → PN	0.370	0.099	0.312	0.052
CN → PN	0.379	0.090	0.392	0.060
PO → CN	0.399	0.097	0.428	0.122
FH → CN	0.470	0.131	0.313	0.038
CK → CN	0.515	0.065	0.342	0.061
PN → CN	0.294	0.063	0.305	0.034

Note: PO: periorbital, FH: forehead, CK: cheeks, PN: perinasal, CN: chin.

Table 3. Significant variations in effective connectivity based on the GC between selected ROIs on the face. The average of all path weights in deceptive and truthful subjects were reported as well.

Source	Target	PWD	PWT	p values
Forehead	Periorbital	0.32	0.57	7×10^{-4}[b]
Chin	Forehead	0.34	0.32	1.9×10^{-2}[a]
Chin	Perinasal	0.31	0.38	3.5×10^{-2}[a]
Periorbital	Forehead	0.23	0.57	4.2×10^{-2}[a]

Note: PWD: path weights in deceptive subjects PWT: path weight in truthful subjects.
[a] $p < 0.05$.
[b] $p < 0.001$.

To assess the performance of the classifiers, we report the sensitivity (true positive rate), specificity (true negative rate), precision (positive predictive value) and F-score (combination of precision and sensitivity), which have been widely used in machine learning literatures (Sokolova and Guy 2009). Table 5 shows the result of this calculation on the three best classifiers and with the three best features which were selected by the ROC feature selection method.

As is shown in table 5, the sensitivity and specificity results in the SVM linear classifier is balanced, which shows high performance of this classification model. This model achieved an accuracy of 0.87, sensitivity of 0.9, specificity of 0.84, precision of 0.85 and F-score of 0.87, which shows the superiority of this model to other classification models in this study.

5. Discussion

Several studies have shown that the sympathetic branch of the autonomous nervous system can affect regional blood flow changes to support and prepare our body for a fight or flight response, which generally corresponds to an increase in muscle irrigation for rapid response such as in the periorbital area that facilitates rapid eye movement (Pavlidis *et al* 2000, Kosonogov *et al* 2017). Although extensive research has been carried out evaluating the performance of ROIs in facial thermal imaging for the detection of deceptive behavior and anxiety, little research has focused on the connection between these regions and the information that might be behind these connections. The initial objective of this study was to identify the network physiology of deceptive anxiety

Table 4. GC feature ranking based on four feature selection methods. The significant links are highlighted by bold.

	T-Test	Relative entropy	ROC	Wilcoxon
1	**FH → PO**	**FH → PO**	**FH →PO**	**FH →PO**
2	**CN →PN**	**CN →FH**	**CN →PN**	PO →PN
3	**PO →FH**	**CN →PN**	**PO →FH**	**CN →PN**
4	**CN →FH**	**PO →FH**	FH →PN	FH →CN
5	PO →PN	PO →PN	CK →CN	CK →PN
6	FH →PN	CK →PN	**CN →FH**	PN →PO
7	CK →CN	PN →CK	PO →PN	**PO →FH**
8	FH →CN	FH →PN	FH →CN	FH →PN
9	CK →PN	CK →PO	CK →PN	CK →CN
10	PN →FH	CN →CK	CK →FH	CN →CK
11	PN →CK	CK →CN	PN →PO	**CN →FH**
12	FH →CK	CK →FH	PN →CK	PN →CN
13	PN →PO	FH →CN	FH →CK	PO →CK
14	PO →CK	FH →CK	PN →FH	CK →PO
15	CK →PO	PN →CN	CN →CK	PO →CN
16	PO →CN	PN →FH	PO →CN	CN →PO
17	CK →FH	PN →PO	CK →PO	CK →FH
18	PN →CN	PO →CK	PO →CK	FH →CK
19	CN →CK	CN →PO	CN →PO	PN →FH
20	CN →PO	PO →CN	PN →CN	PN →CK

Note: PO: periorbital, FH: forehead, CK: cheeks, PN: perinasal, CN: chin.

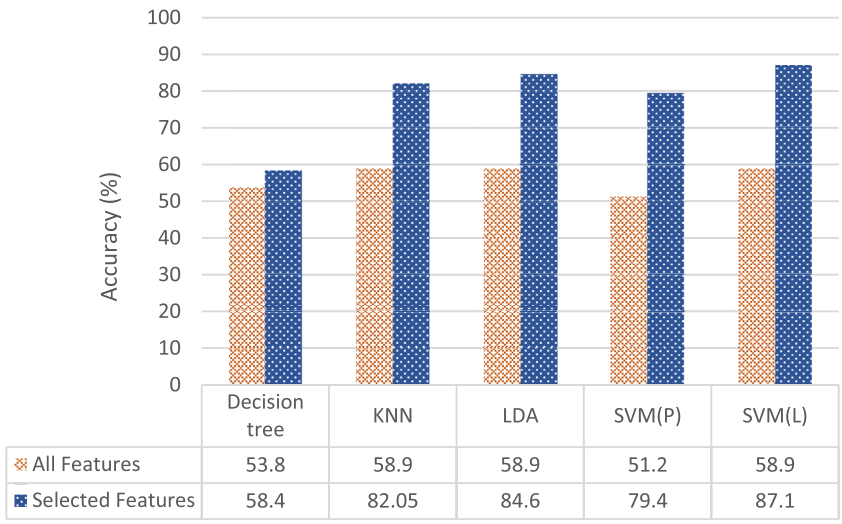

Figure 4. Comparison of classification accuracy rate for all features and the best two features selected with the entropy method. A significant improvement can be seen in the SVM classifier where the classification rate increased from 58.9% to 87.1%.

on the facial superficial temperature patterns which are highly influenced by blood perfusion changes following triggering of the sympathetic nervous system. For this purpose, we used a GC approach to find the effective connectivity among different ROIs on the face.

The results indicate that the redirection of blood flow and temperature is from the lower part of the face to the forehead and periorbital regions. As table 1 shows, there is a significant difference in forehead to periorbital causal connectivity ($p < 0.001$). Chin to forehead, chin to perinasal and periorbital to forehead also shows a significant difference between the two groups ($p < 0.05$). Interestingly, the overall directionality of the temperature on the face seems to originate from lower ROIs such as the chin to upper ROIs such as the periorbital and forehead. Moreover, significant interacting activation of forehead and periorbital areas can be observed in this table. However, the causal connectivity of the forehead to periorbital region is stronger than the other directions. This result is consistent with the physiological background that indicates that the blood flow of the whole face will increase after fight or flight stimulation through the carotid artery (Naqvi and Hanh 2009).

Table 5. This table reports the percentage of accuracy by the three best classifiers with our selected features. In addition to the accuracies, it reports the sensitivity, specificity, precision and F-score to assess the classifier performance more effectively.

Classifier	Accuracy (%)	Sensitivity	Specificity	Precision	F-Score
KNN	82.05	0.9	0.736	0.782	0.837
LDA	84.6	0.9	0.789	0.818	0.857
SVM Linear	87.1	0.9	0.842	0.857	0.878

Moreover, classification was performed to highlight the discriminatory power of connectivity features. The preliminarily results with all features show a successful classification rate of 67.1%. We further improved our classification rate to 87.1% by employing feature selection procedures. The results of our work support our assumption that the fight or flight response leads to quick blood flow changes in the superficial blood vessels of the face. The findings of this investigation complement those of some earlier studies in this field (Tsiamyrtzis 2007, Shastri *et al* 2009).

Due to the heat capacity of skin tissue, skin blood flow is assumed to be about 200 ml/100 g tissue min; the temperature response to a step change in blood flow will exhibit an exponential curve with a time constant of about 30 s (Kosonogov *et al* 2017). Regarding our data acquisition protocol, we asked eight yes/no questions from every subject, and we allowed 20 s for their response to each question. Our analysis focused on question six, which was most relevant to the crime, and we specifically extracted the GC values based on equation (6) over this entire period (20 s). Therefore, it would follow any intrinsic transient time response of the facial temperature variation to the affective arousal stimuli.

6. Conclusion

The main goal of this study was to identify the dynamic nature of blood flow changes effected by the sympathetic nervous system based on the concept of effective connectivity analysis. Our proposed framework assumes that there are simultaneous vasoconstriction and vasodilation on the facial cutaneous vasculature to prepare the body for response to a stress stimulus. For this purpose, a new facial thermal imaging dataset in a mock crime scenario was collected. Five ROIs on the face were selected and the GC indexes between each pair of ROIs were calculated respectively.

A further study could assess the effect of applying smaller time periods for finding the exact dynamic behaviour of this physiological phenomenon. Previously, utilizing time-delay stability (TDS) between physiological time series has been proposed and employed to detect dynamical interactions during different sleep stages (Ivanov *et al* 2017). We believe this algorithm could effectively help us attain an intuitive grasp of the results by extracting the timing information about the physiological outcomes for activation of fight or flight response on the temperature variations in facial superficial blood vessels.

Furthermore, it would be interesting to assess the 'functional connectivity' as well, to explore the time domain correlation of thermal signals as a further investigation in the future. In addition, beyond the GC time domain method, there are other methods that are mostly in the frequency domain and could identify frequency-dependent causal interactions on the face. Finally, the framework we proposed in this study can be used in other medical thermal imaging research to investigate the physiological mechanisms of any blood flow changes on cutaneous vessels.

Acknowledgments

We would like to acknowledge the valuable help of Dr Ying-Hsang Liu, Honorary Lecturer at the ANU Research School of Computer Science, for constructive comments on the paper. Further, we would like to thank the Iranian Ministry of Science, Research and Technology for funding the study and the Research Center of Intelligent Signal Processing-Tehran-Iran for their support in our data collection phase.

Conflict of interest

The authors declare that there is no conflict of interests regarding the publication of this paper.

ORCID iDs

Amin Derakhshan https://orcid.org/0000-0002-1078-6516
Mohammad Mikaeili https://orcid.org/0000-0002-7245-885X
Ali Motie Nasrabadi https://orcid.org/0000-0002-3702-8547

References

Bellucci G 2017 Effective connectivity of brain regions underlying third-party punishment: functional MRI and Granger causality evidence *Soc. Neurosci.* **12** 124–34

Ben Shakhar G 2002 A critical review of the control questions test (CQT) *Handbook Of Polygraph Testing* ed M Kleiner (London: Academic)

Bressler S L and Seth A K 2011 Wiener–Granger causality: a well established methodology *NeuroImage* **58** 323–9

Buchman T G 2006 Physiologic failure: multiple organ dysfunction syndrome *Complex Systems Science in BioMedicine* pp 631–40

Bullmore E and Sporns O 2009 Complex brain networks: graph theoretical analysis of structural and functional systems *Nat. Rev. Neurosci.* **10** 186

Buijs R M and Van Eden C G 2000 The integration of stress by the hypothalamus, amygdala and prefrontal cortex: balance between the autonomic nervous system and the neuroendocrine system *Prog. Brain Res.* **126** 117–32

Deshpande G and Hu X 2012 Investigating effective brain connectivity from fMRI data *Brain* **2** 91

Derakhshan A, Mohammad M, Mohammad A K and Amin M 2014 Preliminary study on facial thermal imaging for stress recognition *Proc. 10th Int. Conf. Intelligent Environments* pp 66–73

Duggento A 2016 Globally conditioned Granger causality in brain–brain and brain–heart interactions: a combined heart rate variability/ultra-high-field (7 T) functional magnetic resonance imaging study *Phil. Trans. R. Soc.* **374** 2067

Faes L and Sameshima K 2014 Assessing connectivity in the presence of instantaneous causality *Methods in Brain Connectivity Inference through Multivariate Time Series Analysis* ed K Sameshima, L A Baccala (Boca Raton, FL: CRC Press) pp 87–112

Fawcett T 2006 An introduction to ROC analysis *Pattern Recognit. Lett.* **27** 861–74

Friston K 2011 Functional and effective connectivity: a review *Brain Connect.* **1.1**, pp 13–36

Friston K, Moran R and Seth A K 2013 Analysing connectivity with Granger causality and dynamic causal modelling *Curr. Opin. Neurobiol.* **23** 172–8

Gane L, Power S, Kushki A and Chau T 2011 Thermal imaging of the periorbital regions during the presentation of an auditory startle stimulus *PLoS One* **6**

Granger C 1969 Investigating causal relations by econometric models and cross-spectral methods *Econometrica* 424–38

Henry T and Gates K 2017 Causal search procedures for fMRI: review and suggestions *Behaviormetrika* **44** 424–38

Henson R and Lucio C 2004 The MATLAB bioinformatics toolbox *Encyclopedia of Genetics, Genomics, Proteomics and Bioinformatics* (New York: Wiley)

Hyvarinen A and Smith S 2013 Pairwise likelihood ratios for estimation of non-Gaussian structural equation models *Mach. Learn. Res.* **14** 111–52

Hyvärinen A, Zhang K, Shimizu S and Hoyer P 2010 Estimation of a structural vector autoregression model using non-gaussianity *J. Mach. Learn. Res.* **11** 1709–31

Ioannou S, Gallese V and Merla A 2014 Thermal infrared imaging in psychophysiology: potentialities and limits *Psychophysiology* **51** 951–63

Ivanov P C, Kang K L, Aijing L and Ronny P B 2017 Network physiology: from neural plasticity to organ network interactions *Emergent Complexity from Nonlinearity, in Physics, Engineering and the Life Sciences* pp 145–65

Ivanov P C, Liu K K and Bartsch R P 2016 Focus on the emerging new fields of network physiology and network medicine *New J. Phys.* **18.10** 100201

Jacobs G D 2001 The physiology of mind–body interactions: the stress response and the relaxation response *J. Altern. Complement. Med.* **7** 83–92

Jacoby W G 2000 Loess:: a nonparametric, graphical tool for depicting relationships between variables *Elect. Stud.* **19** 577–613

Kirk R 2007 *Statistics: An Introduction* (Belmont, CA: Thomson/Wadsworth)

Kosonogov V *et al* 2017 Facial thermal variations: a new marker of emotional arousal *PloS One* **12**

Kullback S 1987 The Kullback–Leibler distance *Am. Stat.* 340–1

Lacroix L, Simona S, Heidbreder C A and Feldon J 2000 Differential role of the medial and lateral prefrontal cortices in fear and anxiety Behavioral Neuroscience **114** 1119–30

LeDoux J 2007 The amygdala *Curr. Biol.* **17** R868–74

Li S, Liao C and Kwok J 2006 Gene feature extraction using t-test statistics and kernel partial least squares *Lecture Notes in Computer Science* pp 11–20

Marrelec G *et al* 2006 Partial correlation for functional brain interactivity investigation in functional MRI *NeuroImage* **32** 228–37

Merla A *et al* 2008 Comparison of thermal infrared and laser doppler imaging in the assessment of cutaneous tissue perfusion in scleroderma patients and healthy controls *Int. J. Immunopathol. Pharmacol.* **21.3** 679–86

Moorman J R, Douglas E L and Ivanov P C 2016 Early detection of sepsis—a role for network physiology *Crit. Care Med.* **44.5** e312–3

Naqvi T Z and Hanh K 2009 Cerebrovascular mental stress reactivity is impaired in hypertension *Cardiovasc. Ultrasound* **7.1** 32

Pavlidis I and Levine J 2002 *Thermal Facial Screening for Deception Detection* (Piscataway, NJ: IEEE)

Pavlidis I *et al* 2012 Fast by nature-how stress patterns define human experience and performance in dexterous tasks *Sci. Rep.* **305**

Pavlidis I, Levine J and Baukol P 2000 *Thermal Imaging for Anxiety Detection* (Piscataway, NJ: IEEE)

Pollina A, Stuart M and Robert G 2015 Hemifacial skin temperature changes related to deception *Int. J. Glob. Res. Comput. Sci.* **6**

Porta A and Faes L 2016 Wiener–Granger causality in network physiology with applications to cardiovascular control and neuroscience *Proc. IEEE* **104.2** 282–309

Prendergast P 2013 Anatomy of the face and neck *Cosmetic Surgery* (Berlin: Springer) pp 29–45

Puri L *et al* 2005 *Stresscam: Non-Contact Measurement of Users' Emotional States Through Thermal Imaging* (Portland, OR: ACM) pp 1725–172

Rajoub B A and Zwiggelaar R 2014 Thermal facial analysis for deception detection *IEEE Trans. Information Forensics and Security* **9** 1015–23

Ren P 2017 Gait influence diagrams in Parkinson's disease *IEEE Trans. Neural Syst. Rehabil. Eng.* pp 1257–67

Rissanen J 1989 Stochastic complexity in statistical inquiry *World Sci.*

Schiatti L, Nollo G, Rossato G and Faes L 2015 Extended Granger causality: a new tool to identify the structure of physiological networks *Physiol. Meas.* **36** 827–43

Seth A K, Barrett A B and Barnett L 2015 Granger causality analysis in neuroscience and neuroimaging *Neurosci. J.* **35** 3293–7

Shastri D, Merla A, Tsiamyrtzis P and Pavlidis I 2009 Imaging facial signs of neurophysiological responses *IEEE Trans. Biomed. Eng.* 477–84

Smith S M, Miller K M, Salimi-Khorshidi G, Webster M, Beckmann C F, Nichols T E, Ramsey J D and Woolrich M W 2011 Network modelling methods for FMRI *Neuroimage* **54** 875–91

Sokolova M and Guy L 2009 A systematic analysis of performance measures for classification tasks *Inf. Process. Manage.* **45.4** 427–37

Ramsey J D, Sanchez-Romero R and Glymour C 2014 Non-Gaussian methods and high-pass filters in the estimation of effective connections *Neuroimage* **84** 986–1006
Tomasi C and Kanade T 1991 Detection and tracking of point features *Technical Report* CMU-CS-91-132
Tsiamyrtzis P, Dowdall J, Shastri D, Pavlidis I T, Frank M G and Ekman P 2007 Imaging facial physiology for the detection of deceit *Int. J. Computer Vision* **71** 197–214
Viola P and Jones M 2001 Rapid object detection using a boosted cascade of simple features *Comput. Vis. Pattern Recognit.*
Wilhelmsen I 2000 Brain-gut axis as an example of the bio-psycho-social model *Gut* **47** (Suppl. 4) iv5–iv7
Yuen T 2009 *Detection and Classification of Stress Using Thermal Imaging Technique* (Bellingham, WA: SPIE) pp 1–9
Zhu Z, Tsiamyrtzis P and Pavlidis I 2007 Forehead thermal signature extraction in lie detection *EMBS 2007. 29th Annual Int. Conf. of the IEEE*